

SEISMIC WAVES IN A BOREHOLE — A REVIEW

M.N. Toksöz, C.H. Cheng and M.E. Willis

Earth Resources Laboratory
Department of Earth and Planetary Sciences
Massachusetts Institute of Technology
Cambridge, MA 02139

ABSTRACT

The propagation of seismic waves in an open borehole is reviewed. The principal wave types are the refracted P and S waves and the two guided waves — pseudo-Rayleigh and Stoneley. The dispersion properties of the guided waves are analyzed. An efficient method of computing synthetic microseismograms is described. The relative effects of the borehole, fluid and formation properties on the propagation characteristics of the different wave types are discussed.

INTRODUCTION

Full waveform acoustic logging is rapidly emerging as an important technique for formation evaluation and for seismic exploration. Borehole measurements of compressional and shear wave velocities and attenuations define formation properties and are used for the modeling and interpretation of seismic reflection and Vertical Seismic Profiling (VSP) data.

In conventional sonic logging a tool may contain one or two sources and a pair of receivers. Only the time-delay (or moveout) of the compressional headwave is recorded and the slowness (inverse of velocity) calculated. With the full waveform acoustic logging tools the entire microseismogram at each receiver is recorded digitally. These new digital tools generally have a longer (8 to 60 ft) source/receiver separation than is commonly used in conventional borehole compensated sonic logging (5 ft). With a combination of multiple sources and receivers, as many as 60 or more records of data can now be obtained at each depth. Thus a large volume of data is generated for even a shallow well. There is more information on these new digital logs than has previously been utilized. Engineering technology has moved ahead of log interpretation. The purpose of this research project is to develop methods for the interpretation and utilization of these data.

At MIT, research on full waveform acoustic logs has been concentrated in three areas:

- (1) Understanding the propagation of elastic waves in the complex environment of the borehole.
- (2) Determining formation P and S wave velocity and attenuation from the data in an efficient manner.

- (3) Extracting additional information about formation properties from the logs directly or by correlation with other logs.

This volume contains detailed technical reports on work that was performed in the past year under the Full Waveform Acoustic Logging Consortium. To understand how these papers fit into the overall program, it is necessary to review briefly the previous developments in full waveform acoustic logging and to introduce the terminology that is used in the reports.

WAVE TYPES IN A BOREHOLE

The borehole environment is complex. A logging sonde hangs in the center of a fluid-filled cylindrical borehole (Figure 1). Waves generated by the source propagate through the fluid (mud) and surrounding formation. In particular, the borehole acts as a very efficient waveguide for the propagation of elastic waves. Several authors have investigated this problem with various degrees of geometrical complexity. Biot (1952), Somers (1953), and Peterson (1974) have worked on analytical solutions of the dispersion characteristics of guided waves in the borehole. Wyatt (1979) and Cheng and Toksöz (1980, 1981) have extended their analyses to include the effects of the logging tool in the borehole. Numerical simulation of the acoustic logs has been attempted by White (1967), White and Zechman (1968), Rosenbaum (1974), Tsang and Rader (1979), Cheng and Toksöz (1980, 1981), Paillet (1980, 1982), and Paillet and White (1982). White and Tongtaow (1981) have extended the analysis to include transversely anisotropic formations while other authors have generated cylindrically layered models (Schoenberg *et al.*, 1981; Cheng *et al.*, 1981; Baker, 1981; Tubman *et al.*, 1982). Willis *et al.* (1982) have examined the effects of elliptic boreholes and decentralized tools upon the waveforms. Schoenberg *et al.* (1981) and Chen (1982) have used scale models to study the borehole wave propagation problem.

For the simple case of a fluid-filled borehole in a formation where both P and S wave velocities are higher than fluid velocity, there are essentially four types of elastic waves which propagate: two headwaves and two guided waves. The well known P wave begins as a compressional wave in the borehole fluid, is critically refracted into the formation as a P wave, and then is refracted back into the fluid as a compressional wave. The so-called "S-wave" begins as a compressional wave in the borehole fluid, is critically refracted into the formation as an S wave, and is refracted back into the fluid as a compressional wave.

Between the P and S headwave arrivals there exists a ringy packet called the leaky or PL mode (Cheng and Toksöz, 1980). The classic PL wave (Phinney, 1961) in a water layer over a half space is an inhomogeneous wave. Paillet and White (1982) have studied the leaky mode in the borehole by examining its plane geometry analog — a fluid layer trapped between two solid half-spaces. They have shown that in this case the leaky mode propagates at a velocity very close to the formation compressional wave velocity. Its phase velocity decreases with increasing frequency. The leaky mode amplitude and hence the appearance of the P-wave train varies strongly with changing Poisson's ratio.

The guided waves are generally dispersive. They arrive after the S wave. They have larger amplitudes and longer durations than either the P or the S wave. Their properties can best be studied by examining their dispersion characteristics. In the following section, a brief review of the dispersion relationships of the guided waves is given, starting from the basic equations. This development will follow the work of Biot (1952) and will use the same notation as Cheng *et al.* (1982).

Dispersion Characteristics of Guided Waves

Given an open borehole with radius R, filled with fluid and surrounded by a homogeneous formation, the wave propagation along the z-axis can be expressed in terms of displacement potentials, φ and ψ .

In cylindrical coordinates, the radial displacement and stress are:

$$u = \frac{\partial \varphi}{\partial r} - \frac{\partial \psi}{\partial z} \quad (1)$$

$$\sigma = \rho \left[\frac{\nu}{1-\nu} \frac{\partial^2 \varphi}{\partial r^2} + 2\mu \left(\frac{\partial^2 \varphi}{\partial r^2} - \frac{\partial^2 \psi}{\partial r \partial z} \right) \right] \quad (2)$$

where ν = Poisson's ratio, μ = shear modulus and ρ = density.

The equations of motion are:

$$\frac{\partial^2 \varphi}{\partial r^2} + \frac{1}{r} \frac{\partial \varphi}{\partial r} + \frac{\partial^2 \varphi}{\partial z^2} = \frac{1}{\alpha^2} \frac{\partial^2 \varphi}{\partial t^2} \quad (3)$$

and

$$\frac{\partial^2 \psi}{\partial r^2} + \frac{1}{r} \frac{\partial \psi}{\partial r} - \frac{\psi}{r^2} + \frac{\partial^2 \psi}{\partial z^2} = \frac{1}{\beta^2} \frac{\partial^2 \psi}{\partial t^2} \quad (4)$$

where α and β are compressional and shear wave velocities.

For the given geometry, the solutions in the solid and fluid are simplified greatly. Taking into account the radiation condition, the solutions for the potentials in the solid are:

$$\varphi = AK_0(lr) e^{ik(z-ct)} \quad (5)$$

and

$$\psi = BK_1(mr) e^{ik(z-ct)} \quad (6)$$

where k is the wave number, c is the phase velocity, and

$$l^2 = k^2 \left(1 - \frac{c^2}{\alpha^2} \right)$$

$$m^2 = k^2 \left(1 - \frac{c^2}{\beta^2} \right)$$

α and β are compressional and shear wave velocities, respectively.

In the fluid, where regular behavior is imposed at $\tau = 0$, the scalar potential is:

$$\varphi_f = CI_0(f\tau) e^{ik(z-ct)} \quad (7)$$

where

$$f^2 = k^2 \left(1 - \frac{c^2}{\alpha_f^2}\right)$$

α_f is the velocity and ρ_f is the density of the fluid.

The pressure, P_f , and radial displacement, u_f in the fluid are:

$$P_f = C\rho_f k^2 c^2 I_0(f\tau) e^{ik(z-ct)} = -\sigma_f \quad (8)$$

and

$$u_f = Cf I_1(f\tau) e^{ik(z-ct)} \quad (9)$$

In the solid, radial displacement, u and radial stress, σ are given by:

$$u = [AlK_0'(lr) - ikBK_1(mr)] e^{ik(z-ct)} \quad (10)$$

and

$$\sigma = \left\{ \rho \frac{\nu}{1-\nu} (-k^2 c^2) AK_0(lr) + 2\rho\beta^2 [Al^2 K_0''(lr) - ikmBK_1'(mr)] \right\} e^{ik(z-ct)} \quad (11)$$

At the borehole interface ($\tau = R$) the boundary conditions require the continuity of radial displacement and stress, and the vanishing of the tangential stress, τ , in the solid. The latter condition is given by:

$$\tau = \{\rho(-k^2 c^2)BK_1(mR) + 2\rho\beta^2 [ikAlK_0'(lR) + k^2 BK_1(mR)]\} e^{ik(z-ct)} = 0 \quad (12)$$

which gives

$$k^2 BK_1(mR) = \frac{2\beta^2}{c^2 - 2\beta^2} ikAlK_0'(lR) \quad (13)$$

Using equations (8-13) in the boundary conditions and carrying out the algebra, the results reduce to:

$$\frac{lc^2 K_1(lR)}{2\beta^2 - c^2} A - f I_1(fR) C = 0 \quad (14)$$

$$\rho \left\{ \frac{2\beta^2 - c^2}{c^2} K_0(lR) + \frac{2\beta^2 lm K_1(lR)}{k^2 (c^2 - 2\beta^2)} \left[\frac{1}{mR} + \frac{2\beta^2 K_0(mR)}{c^2 K_1(mR)} \right] \right\} A + \rho_f I_0(fR) C = 0 \quad (15)$$

For this system of equations to have a non-trivial solution, the determinant of the coefficients (A , C) must be equal to zero. This gives the following period equation:

$$\frac{I_0(fR)}{I_1(fR)} + \frac{f\rho}{l\rho_f} \left\{ \left(\frac{2\beta^2}{c^2} - 1 \right)^2 \frac{K_0(lR)}{K_1(lR)} - \frac{2\beta^2 l m}{k^2 c^2} \left[\frac{1}{mR} + \frac{2\beta^2}{c^2} \frac{K_0(mR)}{K_1(mR)} \right] \right\} = 0 \quad (16)$$

The phase ($c = \frac{\omega}{k}$) and group ($U = \frac{d\omega}{dk} = c + k \frac{dc}{dk}$) velocities of the guided waves can be calculated as a function of wavenumber k or frequency ω by solving the period equation (16). A set of such curves is shown in Figure 2.

The Pseudo-Rayleigh Wave

There are two separate guided wave types. The first group of guided waves is known as the "pseudo-Rayleigh" waves (Cheng and Toksöz, 1981; Tsang and Rader, 1979). They are also called "reflected conical" waves by Biot (1952) and "normal modes" by Paillet (1980) and Schoenberg *et al.* (1981). These waves have an infinite number of modes, each with a low frequency cut-off. Their amplitudes decay radially away from the borehole wall in the solid and are oscillatory in the fluid. Their phase velocities are bounded by the formation shear wave velocity from above and the borehole fluid velocity from below. The group velocities dip below the fluid velocity. The phase and group velocities for the two modes are shown in Figure 2 as a function of frequency. At the low frequency end there is a cut-off, below which these waves cannot propagate and are rapidly attenuated. For the lowest mode the cut-off frequency is about 10 kHz or higher and is strongly dependent on borehole radius. It is evident, from the steepness of the dispersion curves, that the pseudo-Rayleigh wave is very dispersive. In a microseismogram, it will arrive as a nearly monochromatic wave train, lasting from just after the refracted S wave to after the Stoneley wave arrival, with an Airy phase at about 0.8 times the fluid velocity. The pseudo-Rayleigh wave can only exist as a proper guided wave in formations where the shear wave velocity is higher than the borehole fluid velocity.

The Stoneley Wave

The second type of guided wave is the Stoneley wave. Its amplitude decays exponentially both in the fluid and in the formation away from the fluid/rock interface. It has very little dispersion. As shown in Figure 2, its phase and group velocities are slower than the compressional velocity of the borehole fluid. The Stoneley wave is essentially a compact pulse and will arrive at a time slightly later than what would be expected for a direct fluid arrival. The wave is especially prominent when the receiver is placed close to the borehole wall. It is important to note that when the shear velocity of the formation is slower than the borehole fluid velocity, the Stoneley wave can still exist but will propagate with a phase velocity lower than the shear velocity.

From the period equation, it is clear that the dispersion curves for both the pseudo-Rayleigh and the Stoneley waves are functions of the wavenumber times the borehole radius. In terms of frequency, for a small radius borehole, the dispersion curves will be shifted to higher frequencies, and vice versa for a large radius borehole. Owing to the highly dispersive nature of the pseudo-Rayleigh wave and the existence of a cut-off frequency for each of its modes, the radius of the borehole plays a role that is as important as the source frequency in the relative excitation of the different modes of the pseudo-

Rayleigh wave. In contrast, because the Stoneley wave is not very dispersive and does not have a cut-off frequency, its excitation is less affected by the borehole radius.

In order to determine the relative importance of guided waves it is necessary to examine their amplitude response curves (Paillet and White, 1982). Once the phase velocities are obtained from equation (16), these values can be substituted into equations (14) and (15) to obtain the constant C . Then, using equations (8) or (9), amplitude responses can be obtained in the borehole. In Figure 3, relative amplitudes of the Stoneley and the two lowest modes of pseudo-Rayleigh waves are shown. Note that at low frequencies ($f \leq 10$ kHz), the Stoneley wave amplitudes are larger. At frequencies higher than about 20 kHz, more than one mode of the pseudo-Rayleigh wave will be present.

SYNTHETIC MICROSEISMOGRAMS

The full waveform acoustic logs are controlled by the velocity and attenuation of the different phases and their relative amplitudes. The best way of looking at the combined effect is to synthesize the microseismograms. The pressure response $P(r, z, t)$ in a fluid-filled borehole at an axial distance z and radial distance r from a point isotropic source is given by Cheng *et al.* (1982):

$$P(r, z, t) = \int_{-\infty}^{\infty} S(\omega) e^{-i\omega t} \int_{-\infty}^{\infty} G I_0(fr) e^{ikz} dk \quad (17)$$

where $S(\omega)$ is the Fourier spectrum of the source and G is given by:

$$G = \frac{g K_1(fR) - K_0(fR)}{g J_1(fR) + I_0(fR)} \quad (18)$$

where

$$g = \frac{f \rho}{l \rho_f} \left\{ \left(\frac{2\beta^2}{c^2} - 1 \right)^2 \frac{K_0(lR)}{K_1(lR)} - \frac{2\beta^2 l m}{\omega^2} \left[\frac{1}{mR} + \frac{2\beta^2}{c^2} \frac{K_0(mR)}{K_1(mR)} \right] \right\} \quad (19)$$

The above form is slightly modified from those given in Tsang and Rader (1979) and Cheng and Toksöz (1981) so that the conventions used are consistent with those used in this report.

To generate the synthetic microseismograms, a double numerical integration in k and ω is necessary. The k integration is performed using the discrete wavenumber representation (Bouchon and Aki, 1977; White and Zechman, 1968). An integration interval Δk is equivalent to an infinite distribution of source separated by a distance $L = 2\pi/\Delta k$ apart along the z axis. Thus Δk is chosen such that L is large enough that the first arrivals from neighboring fictitious sources are out of the time window under consideration. The upper limit in the k summation can be determined numerically using a convergence criteria.

To perform the k summation, the singularities have to be removed from the real k axis. This is done by assigning a small imaginary part to the frequency (Rosenbaum, 1974; Bouchon and Aki, 1977; Tsang and Rader, 1979; Cheng and

Toksöz, 1981):

$$\omega = \omega_r + i\omega_i, \quad \omega_i > 0. \quad (20)$$

The effect of the imaginary part can be removed by multiplying the resulting time domain representation of the pressure response by $e^{\omega_i t}$.

The effect of formation and fluid attenuation can be introduced in very much the same way. The transformation is (Anderson *et al.*, 1965):

$$\frac{1}{v_i} \rightarrow \frac{1}{v_i(\omega)} \left[1 + \frac{i}{2Q_i(\omega)} \right] \quad (21)$$

where v_i and Q_i are the formation and fluid body wave velocities and their respective Q 's. For constant Q , the phase velocity dispersion associated with attenuation is given by (Futterman, 1962):

$$\frac{v(\omega_1)}{v(\omega_0)} = 1 + \frac{1}{\pi Q} \ln \left[\frac{\omega_1}{\omega_0} \right]$$

so

$$\frac{1}{v_i(\omega)} \rightarrow \frac{1}{v_i(\omega_0)} \left[1 + \frac{\ln(\omega/\omega_0)}{\pi Q_i} \right] \left[1 + \frac{i}{2Q_i} \right] \quad (22)$$

where ω_0 is the reference frequency at which the velocity v_i is taken. This approach can be easily adapted to frequency dependent attenuation. For full waveform acoustic logging, owing to the relatively narrow frequency range used, the frequency dependence of Q is insignificant.

The type of source used plays an important part in the generation of the synthetic microseismograms. Commonly used sources are: a sinusoid with a decaying exponential envelope (Tsang and Rader, 1979), a Ricker (1977) wavelet, and a Kelly type source (Kelly *et al.*, 1976), which is similar to the derivative of the Ricker wavelet. These sources are described in more detail in the Appendix.

Numerical Examples

With an efficient method of generating synthetic microseismograms, the effects of formation and borehole parameters on the observed waveforms can be investigated numerically. Figure 4 shows an example of a synthetic microseismogram in a typical hard limestone formation. The source used is a relatively broad banded Tsang and Rader source. The source-receiver distance is 8 ft. The P and S wave arrivals are clearly identified. The lower frequency branch of the pseudo-Rayleigh wave, with a group velocity higher than the Stoneley wave velocity, is labeled **a**. There is a slight normal dispersion from low to higher frequencies. The Stoneley wave arrives in a pulse and is labeled **b**. After the Stoneley wave arrival, there is a packet of higher frequency arrival labeled **c**. This corresponds to the Airy phase of the pseudo-Rayleigh wave. Thus, all the characteristics of the waveform are well illustrated and can be properly identified.

Effect of Borehole Radius

Plotted in Figure 5 are three synthetic microseismograms generated using the same formation and fluid parameters but different borehole radii. Figure 5a shows the case of a very small borehole (radius = 1.8 in). The P and S arrivals are not prominent. The pseudo-Rayleigh wave arrival after the S is also of relatively small amplitude. The major arrival is the Stoneley wave with a group velocity slightly lower than the P wave velocity of the fluid. This behavior is expected since for small borehole radius, the dispersion curves are shifted to higher frequencies. Thus the majority of the energy of the source is below the cutoff frequency of the fundamental mode of the pseudo-Rayleigh wave. On the other hand, since the Stoneley waves do not have a low frequency cutoff, they are excited by all the energy in the source. Furthermore, since the amplitudes of the Stoneley waves decay exponentially in the fluid away from the boundary, a smaller borehole radius means that the receiver is closer to the boundary, thus detecting a larger amplitude Stoneley wave.

For contrast, the case of a large radius (4 in) borehole is shown in Figure 5b. The P and S arrivals are still not prominent. However, the pseudo-Rayleigh wave arrivals after the S are larger in amplitude. The Stoneley wave arrival is smaller than the previous case. The major arrival in this case is the Airy phase coming in after the Stoneley waves.

The case of the intermediate hole size (radius = 2.64 in) is shown in Figure 5c. The waveform of the microseismogram is entirely different from the previous two cases. There is significant energy in the leaky mode between the P and S arrivals. The amplitudes of the pseudo-Rayleigh and Stoneley waves are comparable. Stoneley waves arrive in the middle of the pseudo-Rayleigh wave train and are visible when they disturb the coherency of the wave train. There is a decrease in frequency at the Stoneley wave arrival.

Effect of Formation Poisson's Ratio

The effects of the Poisson's ratio of the formation on the microseismograms are shown in Figure 6. Here, all the parameters except the P wave velocity of the formation are kept constant. The formation Poisson's ratio used in Figure 6a, b and c are 0.32, 0.26 and 0.10, respectively. The figures show that the microseismograms are generally similar. The major difference among the three cases is the relative amplitudes of the P leaky modes. As the Poisson's ratio of the formation decreases, the amplitude of the leaky mode also decreases. This behavior is expected theoretically. Thus, the relative prominence of the P wave leaky mode could give us a good indication of the Poisson's ratio of the formation. A similar observation in "soft" formations, where the shear wave velocities are lower than the borehole fluid velocity, is given in Paper 2 of this technical report.

SENSITIVITY OF GUIDED WAVES TO FORMATION AND FLUID PROPERTIES

When the formation P wave velocity was changed, while all other parameters remained constant, the P wave train changed significantly. Yet no noticeable change occurred in the guided wave, as shown in Figure 6. The questions that arise naturally then are:

- (1) Are the guided waves sensitive to formation properties, and if so, which ones?
- (2) Do the properties of the borehole fluid (drilling mud) significantly affect the properties of the guided waves?

The answers to both of these questions are affirmative, and among the formation properties, the shear wave velocity and attenuation play much more significant roles than their compressional wave counterparts.

Partition Coefficients

The relative effects of formation and fluid parameters on the velocity and attenuation of the guided wave can be evaluated using partial derivatives and energy "partition coefficients". Following the standard seismological procedures (Anderson and Archambeau, 1964; Anderson *et al.*, 1965; Cheng *et al.*, 1982), five partition coefficients can be defined for each mode of the pseudo-Rayleigh and the Stoneley wave. These are the normalized partial derivatives of the phase velocity of the guided wave with respect to the formation and fluid body wave velocities and densities. More explicitly, they are $\frac{\alpha}{c} \frac{\partial c}{\partial \alpha}$, $\frac{\beta}{c} \frac{\partial c}{\partial \beta}$, $\frac{\alpha_f}{c} \frac{\partial c}{\partial \alpha_f}$, $\frac{\rho}{c} \frac{\partial c}{\partial \rho}$, and $\frac{\rho_f}{c} \frac{\partial c}{\partial \rho_f}$. The partial derivatives are taken either at a fixed frequency ω or at a fixed wavenumber k . In the following analysis, they are taken at a fixed wavenumber k .

The partition coefficients can be obtained by numerically differentiating the dispersion curves, or, preferably, by the variational principle approach. The latter is described in detail by Cheng *et al.* (1982). Only the results will be summarized here for the sake of brevity.

Let the radial and axial displacements, u and w , be

$$u = u_1(r) e^{ik(z-ct)} \quad (23a)$$

$$w = iu_2(r) e^{ik(z-ct)}, \quad (23b)$$

Holding the formation and fluid densities constant, the partition coefficients can be written as:

$$\frac{\alpha}{c} \frac{\partial c}{\partial \alpha} = \frac{1}{2\omega^2 I} \int_R^\infty (\lambda + 2\mu) \left(\frac{\partial u_1}{\partial r} + \frac{u_1}{r} - ku_2 \right)^2 r dr, \quad (24a)$$

$$\frac{\beta}{c} \frac{\partial c}{\partial \beta} = \frac{1}{\omega^2 I} \int_0^{\infty} \mu \left[\left(\frac{\partial u_1}{\partial r} \right)^2 + \left(\frac{u_1}{r} \right)^2 + k^2 u_2^2 - \left(\frac{\partial u_1}{\partial r} + \frac{u_1}{r} - k u_2 \right)^2 + \frac{1}{2} \left(k u_1 + \frac{\partial u_2}{\partial r} \right)^2 \right] r dr, \quad (24b)$$

$$\frac{\alpha_f}{c} \frac{\partial c}{\partial \alpha_f} = \frac{1}{2\omega^2 I} \int_0^R \lambda \left(\frac{\partial u_1}{\partial r} + \frac{u_1}{r} - k u_2 \right)^2 r dr, \quad (24c)$$

where

$$I = \frac{1}{2} \int_0^{\infty} \rho (u_1^2 + u_2^2) r dr. \quad (25)$$

and λ and μ are the Lamé constants. If the Lamé constants are held constant, the partial derivatives of the formation and fluid densities with respect to the phase velocity of the guided waves are given by:

$$\frac{\rho}{c} \frac{\partial c}{\partial \rho} = -\frac{\rho}{4I} \int_0^{\infty} (u_1^2 + u_2^2) r dr, \quad (26a)$$

$$\frac{\rho_f}{c} \frac{\partial c}{\partial \rho_f} = -\frac{\rho_f}{4I} \int_0^R (u_1^2 + u_2^2) r dr. \quad (26b)$$

A byproduct of the variational principle approach is that the group velocity U of the guided wave can be expressed in terms of integrals. This gives a much more stable method of numerically evaluating the group velocity than taking the derivative of the phase velocity dispersion curve. The group velocity U is given by

$$U = \frac{1}{2cI} \int_0^{\infty} \left[\mu u_1 \left(u_1 + \frac{\partial u_2}{k \partial r} \right) + (\lambda + 2\mu) u_2^2 - \frac{\lambda}{k} u_2 \left(\frac{\partial u_1}{\partial r} + \frac{u_1}{r} \right) \right] r dr. \quad (27)$$

All of the above integrals can be evaluated by first solving the period equation (16) for the guided wave mode of interest and then evaluating the displacement functions u_1 and u_2 . Specifically, the displacement functions are:

in the fluid ($r \leq R$)

$$u_1 = f C I_1(f r), \quad (28a)$$

$$u_2 = k C I_0(f r); \quad (28b)$$

and in the solid ($r \geq R$)

$$u_1 = -l A K_1(l r) - i k B K_1(m r), \quad (29a)$$

$$u_2 = k A K_0(l r) + i m B K_0(m r). \quad (29b)$$

The constants A and B are related by equation (13). A and C are related by the

solution to the period equation (16).

Attenuation

An important use of the partition coefficients is the determination of the contribution of formation and fluid body wave attenuation to the attenuation of the pseudo-Rayleigh and Stoneley waves. For a given guided wave mode, the attenuation, Q_g^{-1} , can be expressed as

$$\frac{1}{Q_g} = \frac{\alpha}{c} \frac{\partial c}{\partial \alpha} \frac{1}{Q_\alpha} + \frac{\beta}{c} \frac{\partial c}{\partial \beta} \frac{1}{Q_\beta} + \frac{\alpha_f}{c} \frac{\partial c}{\partial \alpha_f} \frac{1}{Q_f}, \quad (30)$$

neglecting second order and higher terms in Q^{-1} . Q_α^{-1} , Q_β^{-1} , and Q_f^{-1} are the P and S wave attenuation in the formation and the P wave attenuation in the borehole fluid, respectively; c is the phase velocity of the guided wave.

It should be noted that all partition coefficients are frequency dependent. Thus, their magnitudes depend both on the formation and fluid properties and on frequency.

Numerical Examples

The partition coefficients versus frequency for a typical sandstone formation are plotted in Figure 7. Figure 7a is for the fundamental mode of the pseudo-Rayleigh wave and Figure 7b is for the Stoneley wave. The partition coefficients for the pseudo-Rayleigh wave are strong functions of frequency. For low frequencies (around the cut-off frequency) the properties of the pseudo-Rayleigh wave are primarily controlled by the shear wave properties of the rock. However, the effect of the borehole fluid increases rapidly with frequency and dominates at higher frequencies. The contribution of the formation P wave properties is negligible at all frequencies.

For the Stoneley wave, the partition coefficients are not a strong function of frequency (Figure 7b). The borehole fluid most strongly affects the Stoneley waves at all frequencies. The contribution from the S wave properties of the rock are small. Once again, the P wave properties of the rock have little effect on the attenuation of the Stoneley waves at all frequencies.

In Figure 8a, the partition coefficients for a "softer" sedimentary rock (e.g., shale or shaly sand) are plotted. The sediment shear wave velocity is lower than the borehole fluid velocity, so the pseudo-Rayleigh wave does not exist. The relative contributions of the fluid and the formation shear wave properties on the Stoneley wave properties are quite different than in the previous case, although the effect of the formation P wave remains insignificant. The effects of the fluid and formation S wave on the Stoneley waves are comparable at very low frequencies. As the frequency increases, the contribution of the formation S wave increases, dominating at high frequencies. This behavior is entirely opposite to the cases with more competent, or "fast" formations.

For the same case, the normalized density derivatives, $\frac{\rho}{c} \frac{\partial c}{\partial \rho}$ and $\frac{\rho_f}{c} \frac{\partial c}{\partial \rho_f}$ are

shown in Figure 8b. Note that in this case the Stoneley wave velocities are also strongly affected by the formation density at higher frequencies. If the formation shear wave velocity can be determined independently (e.g., from the amplitude of the P wave leaky mode), and the fluid properties are known, then the Stoneley wave velocity can be used to determine the formation density.

From the examples shown here, as well as those calculated for other formations (Cheng *et al.*, 1982), the following generalizations can be made regarding the sensitivity of the guided waves to formation and fluid properties:

- (1) The guided waves are most sensitive to formation shear and borehole fluid velocities.
- (2) For "hard" formations (e.g., crystalline rocks, hard limestones and dolomites), the pseudo-Rayleigh waves are sensitive to formation shear wave properties at low frequencies (near the cut-off frequency), but at high frequencies the borehole fluid (mud) effects dominate. For the Stoneley waves, the fluid properties dominate at all frequencies.
- (3) For formations with average sandstone velocities, the sensitivity of the pseudo-Rayleigh wave to formation shear wave velocity becomes more dominant than the "hard" formation case and extends to a wider frequency range. For the Stoneley wave, the effects of the formation shear wave properties become noticeable.
- (4) For low shear wave velocity formations (i.e. $\beta \leq \alpha_f$), the Stoneley waves are very sensitive to formation shear wave velocities and moderately sensitive to formation densities.
- (5) In all cases, the guided waves are *insensitive* to formation P wave velocities.
- (6) In most cases, the relative sensitivities of guided wave velocity and attenuation to formation and borehole fluid properties are frequency dependent. Thus, if data are available from tools with broad band frequency responses, both the formation shear wave and the borehole fluid velocity can be determined from the velocity of the guided waves.
- (7) Given the effects of the borehole fluid velocity and attenuation on the guided waves, it is important to measure these fluid parameters independently, ideally in the well during the logging run, or at the least in the laboratory or the mud pit at the well site.

COMPARISON WITH FIELD DATA

Given the number of parameters (formation P and S wave velocity and attenuation, borehole radius, fluid velocity, formation and fluid density, and source/receiver frequency response) that affect the full waveform acoustic logs, the question arises whether it is possible to use the waveforms in real earth applications. The answer is definitely positive. A practical approach to the use of the synthetic microseismograms for the interpretation of field data requires the following step-by-step procedure. Firstly, obtain the engineering

information such as borehole radius, tool geometry, mechanical properties of the sonde and its source/receiver frequency response. Secondly, obtain as much information (velocity, density, attenuation) about the borehole fluid (drilling mud) as possible. Thirdly, obtain the formation P and S wave velocity using one of the methods described in Paper 6 of this technical report. Finally, put in some approximate values of the P and S wave attenuation. Using these parameters as initial guesses, calculate the synthetic microseismograms. Fine tuning of the parameters can then be made to match the synthetic microseismograms generated with the field data.

Comparisons of field data from two different formations with synthetic microseismograms are presented in Figures 9 and 10. Figure 9a shows the observed microseismogram in a hard limestone formation. The source used has very narrow bandwidth, around 15 kHz. This is typical of the commercial tools in existence at the present time. The waveform has a prominent P wave packet, with a distinct S wave arrival. The pseudo-Rayleigh wave packet immediately following the S wave arrival is large and ringy. There is no distinguishable Stoneley wave arrival. Figure 9b shows the corresponding synthetic microseismogram generated using the formation P and S wave velocity and attenuation determined from the field data (see Paper 6 of this technical report). The agreement between the synthetic and field data is excellent.

Figure 10a shows the observed microseismogram from a "slow" formation where the shear wave velocity is lower than the borehole fluid velocity. The tool used in this data set has a much broader source frequency bandwidth. The P wave and the associated P leaky mode together constitute the large amplitude packet seen in the microseismogram. The Stoneley wave is very low frequency and distinct. As expected, there is no S wave arrival. Figure 10b shows the corresponding synthetic microseismogram. Once again, the agreement between the two is excellent.

Matching the observed and synthetic waveforms for a complete microseismogram is the ultimate test of the accuracy of the formation parameters.

APPENDIX

Commonly Used Sources in Synthetic Microseismograms

The three most commonly used sources in the generation of synthetic microseismograms are: 1) the Tsang and Rader (1979) source; 2) the Ricker (1977) wavelet; and 3) the Kelly source (Kelly *et al.*, 1976). The analytic Fourier frequency spectrum of each is as follows:

(1) Tsang and Rader:

$$S(\omega) = \frac{8\alpha\omega_0(\alpha - i\omega)}{[(\alpha - i\omega)^2 + \omega_0^2]^2} \quad (\text{A1})$$

(2) Ricker wavelet:

$$S(\omega) = \left(\frac{\omega}{\omega_0}\right)^2 e^{-(\omega/\omega_0)^2} \quad (\text{A2})$$

(3) Kelly:

$$S(\omega) = \left(\frac{\pi}{\xi}\right)^{1/2} \omega^3 e^{-\omega^2/4\xi} \quad (\text{A3})$$

In both the Ricker wavelet and the Tsang and Rader source, ω_0 is the center frequency of the source. In the Kelly source, the center frequency is given by $f_{peak} = 0.39\sqrt{\xi}$.

Each source has its own strength and weakness. The Tsang and Rader source is the only one that is both causal and in which the bandwidth can be independently adjusted. The bandwidth is controlled by the parameter α . Both the Ricker wavelet and the Kelly source are zero phase wavelets. A time shift can be applied to make $s(t) \approx 0$ at $t = 0$. The bandwidth of these two sources cannot be adjusted independently of the center frequency. The Tsang and Rader source, however, has a dc offset in its frequency spectrum. For an isotropic point source in the center of the borehole, the Stoneley wave has a large amplitude at low frequencies. Thus the Tsang and Rader source, without any high pass or bandpass filter, will preferentially excite a large amount of Stoneley waves. This problem is magnified when attenuation is introduced. For a constant Q model, attenuation increases linearly with frequency. On the other hand, owing to the ω^2 and ω^3 behavior in the Ricker wavelet and the Kelly source, respectively, these sources do not have the same problem with Stoneley wave generation. In general, these three sources, in combination with a bandpass filter, do an adequate job in mimicking the combined source/receiver response of most tools in use at the present time.

REFERENCES

- Aki, K. and Richards, P., 1980, Quantitative Seismology — Theory and Methods, v.1, Freeman, San Francisco, CA.
- Anderson, D.L. and Archambeau, C.B., 1964, The anelasticity of the earth: J. Geophys. Res., v.69, p.2071-2084.
- Anderson, D.L., Ben-Menahem, A. and Archambeau, C.B., 1965, Attenuation of seismic energy in the upper mantle: J. Geophys. Res., v.70, p.1441-1448.
- Baker, L.J., 1981, The effect of the invaded zone in full waveform acoustic logging: Presented at the 51st Ann. Int. Meeting of the S.E.G., Los Angeles, CA.
- Biot, M. A., 1952, Propagation of elastic waves in a cylindrical bore containing a fluid: J. Appl. Phys., v.23, p.977-1005.
- Bouchon, M. and Aki, K., 1977, Discrete wave-number representation of seismic-source wave fields: Bull. Seism. Soc. Am., v.67, p.259-277.
- Chen, S.T., 1982, The full acoustic wave train in a laboratory model of a borehole: Geophysics, v.47, p.1512-1520.
- Cheng, C.H. and Toksöz, M.N., 1980, Modelling of Full Wave Acoustic Logs: SPWLA 21st Ann. Log. Symp. Trans., Paper J.
- _____, 1981, Elastic wave propagation in a fluid-filled borehole and synthetic acoustic logs: Geophysics, v.46, p.1042-1053.
- Cheng, C.H., Toksöz, M.N., and Willis, M.E., 1982, Determination of in situ attenuation from full waveform acoustic logs: J. Geophys. Res., v.87, p.5477-5484.
- Cheng, C.H., Tubman, K. and Toksöz, M.N., 1981, Propagation of seismic waves in a multilayered borehole: Presented at the 51st Ann. Int. Meeting of the S.E.G., Los Angeles, CA.
- Futterman, W.I., 1962, Dispersive body waves: J. Geophys. Res., v.67, p.5257-5291.
- Kelly, K.R., Ward, R.W., Treitel, S., and Alford, R.M., 1976, Synthetic seismograms: a finite-difference approach: Geophysics, v.41, p.2-27.
- Paillet, F., 1980, Acoustic propagation in the vicinity of fractures which intersect a fluid-filled borehole: SPWLA 21st Ann. Log. Symp. Trans., Paper DD.
- _____, 1982, A comprehensive theory for the interpretation of compressional and shear head waves in boreholes: submitted to Bull. Seis. Soc. Am.
- Paillet, F. and White, J.E., 1982, Acoustic models of propagation in the borehole and their relationship to rock properties: Geophysics, v.47, p.1215-1228.

- Peterson, E.W., 1974, Acoustic wave propagation along a fluid-filled cylinder: J. Appl. Phys., v.45, p.3340-3350.
- Phinney, R.A., 1961, Leaking modes in the crustal waveguide: J. Geophys. Res., v.66, p.1445-1469.
- Ricker, N., 1977, Transient waves in visco-elastic media: Development in Solid Earth Geophysics, v.10, Elsevier, Amsterdam, The Netherlands.
- Rosenbaum, J.H., 1974, Synthetic microseismograms: logging in porous formations: Geophysics, v.39, p.14-32.
- Schoenberg, M., Marzetta, T., Aron, J. and Porter, R., 1981, Space-time dependence of acoustic waves in a borehole: J. Acous. Soc. Am., v.70, p.1496-1507.
- Somers, E.V., 1953, Propagation of acoustic waves in a liquid filled cylindrical hold, surrounded by an elastic solid: J. Appl. Phys. v.24, p.515-521.
- Tsang, L. and Rader, D., 1979, Numerical evaluation of transient acoustic waveform due to a point source in a fluid-filled borehole: Geophysics, v.44, p.1706-1720.
- Tubman, K., Cheng, C.H. and Toksöz, M.N., 1982, Effects of casing on full waveform acoustic logs: Presented at the 52nd Ann. Int. Meeting of the S.E.G., Dallas, TX.
- White, J.E., 1967, The hula log: a proposed acoustic log: SPWLA 8th Ann. Log. Symp. Trans., Paper I.
- White, J.E. and Tongtaow, C., 1981, Cylindrical waves in transversely isotropic media: J. Acous. Soc. Am., v.70, p.1147-1155.
- White, J.E. and Zechman, R.E., 1968, Computed response of an acoustic logging tool: Geophysics, v.33, no.2, pp.302-310.
- Willis, M.E. and Toksöz, M.N., 1982, Automatic P and S velocity determination from full waveform digital acoustic logs: Submitted to Geophysics.
- Willis, M.E., Toksöz, M.N. and Cheng, C.H., 1982, Approximate effects of off-center acoustic sondes and elliptic boreholes upon full waveform logs: Presented at the 52nd Ann. Int. Meeting of the S.E.G., Dallas, TX.
- Wyatt, S.B., 1979, The propagation of elastic waves along a fluid-filled annular region: Master's thesis, University of Tulsa, OK.

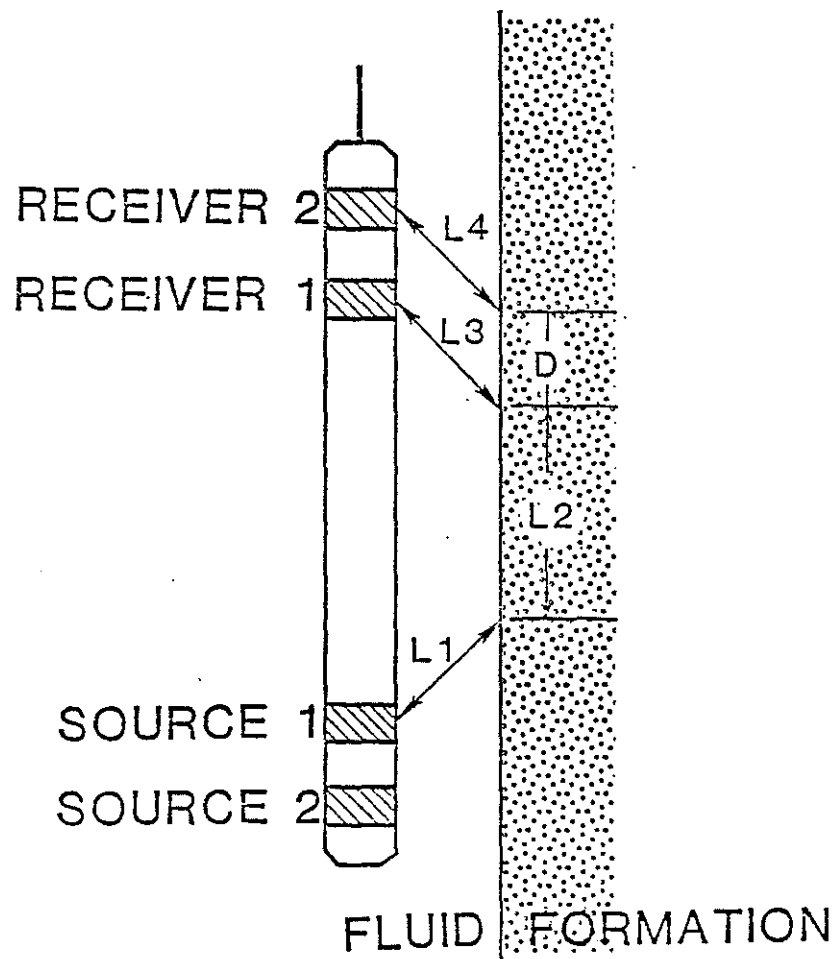


Figure 1: Schematic diagram of a logging tool.

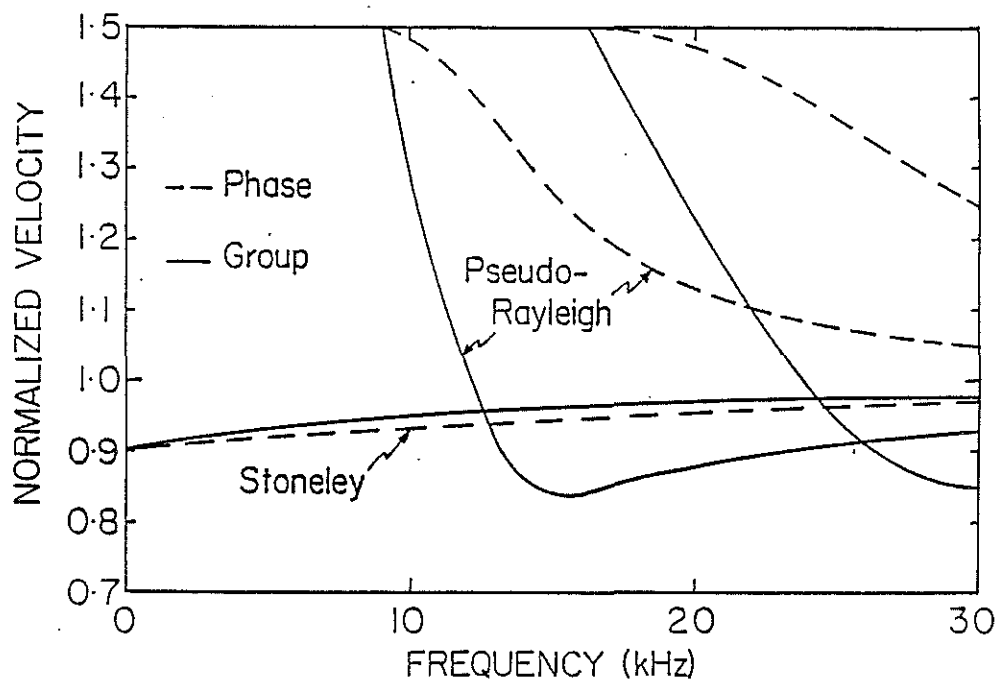


Figure 2: Phase and group velocity dispersion curves for the first two modes of the pseudo-Rayleigh wave and the Stoneley wave in an open borehole in a "hard" formation.

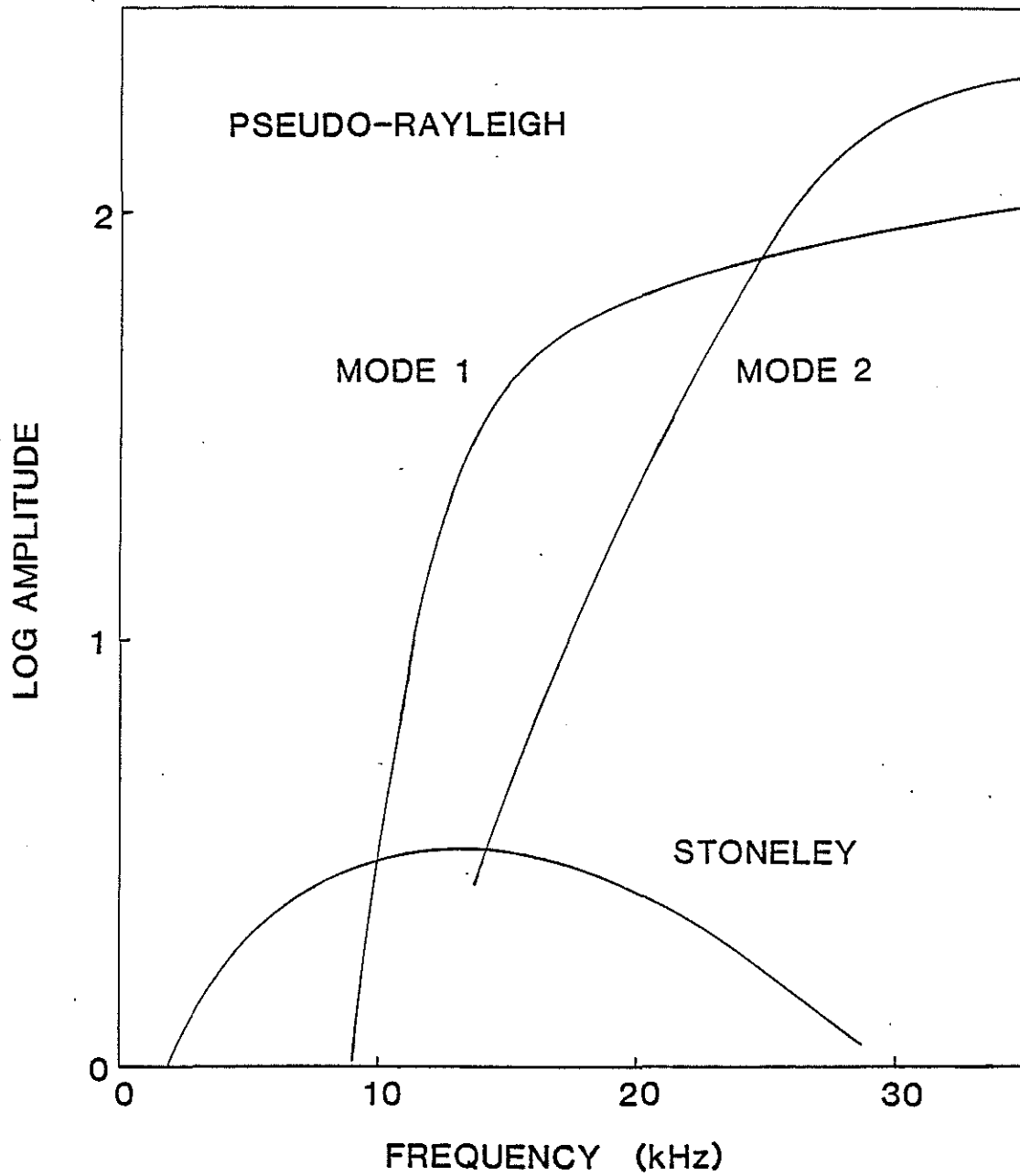


Figure 3: Amplitude response functions of the Stoneley wave and the first two modes of the pseudo-Rayleigh wave in an open borehole in a "hard" formation.

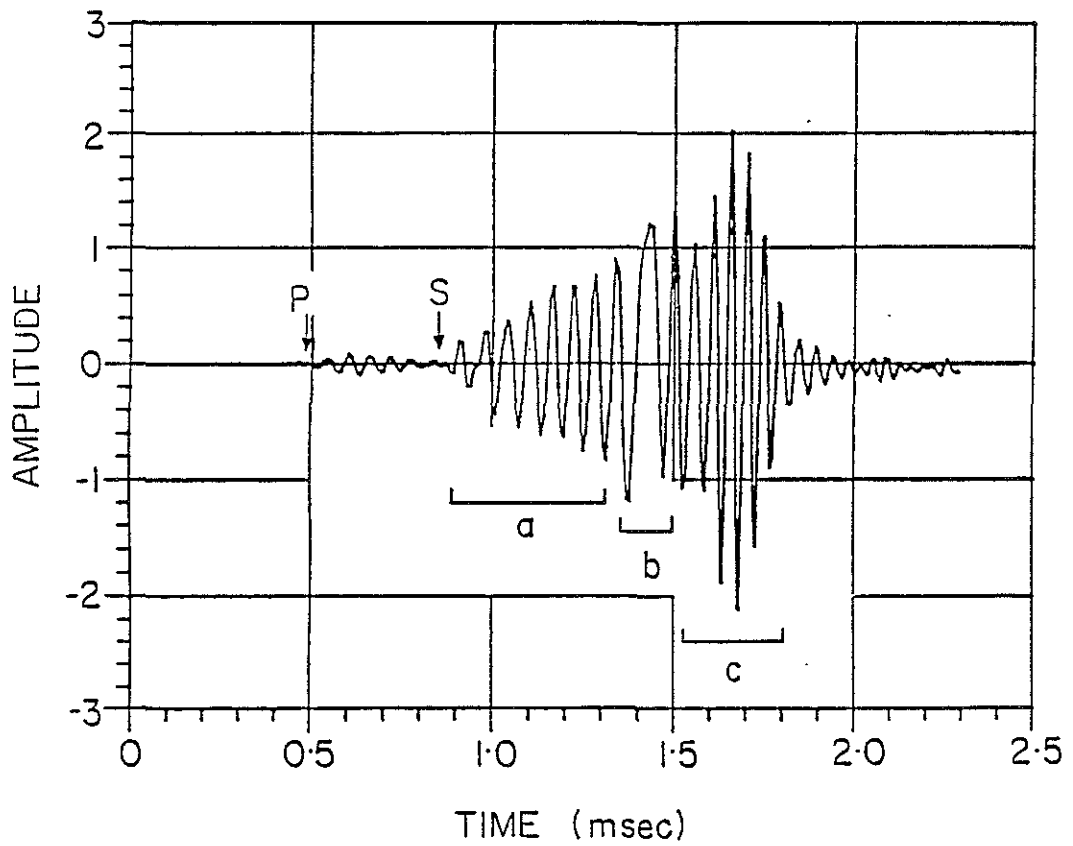


Figure 4: Synthetic microseismogram in an open borehole. The guided wave phases are: (a) the lowest frequency branch of the pseudo-Rayleigh wave; (b) the Stoneley wave; (c) the Airy phase of the pseudo-Rayleigh wave.

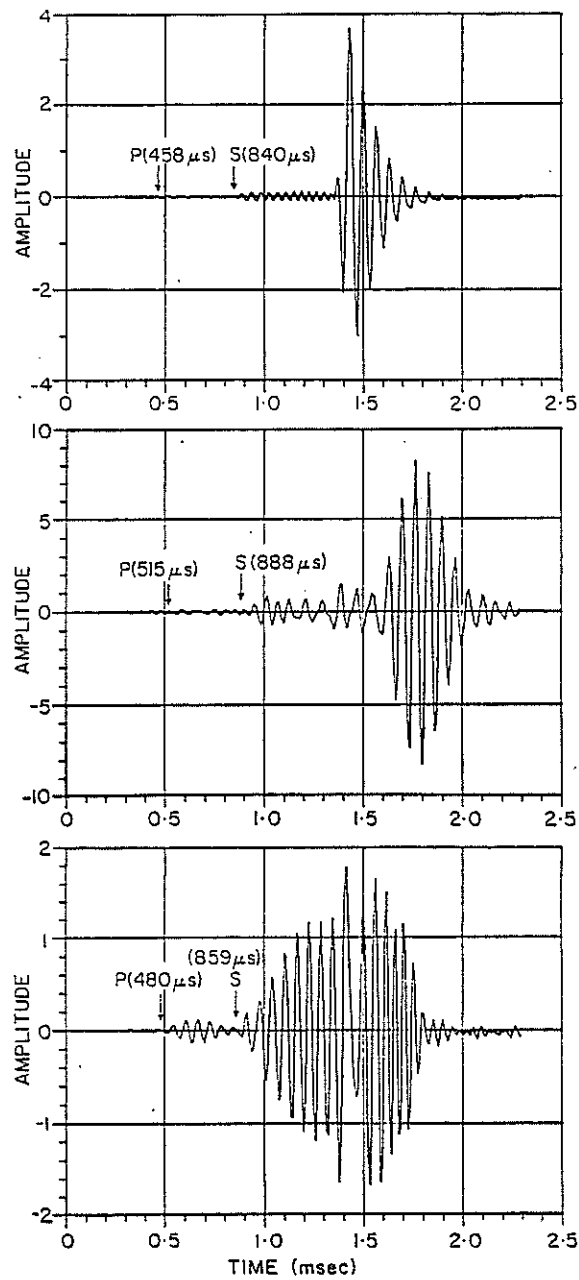


Figure 5: Synthetic microseismograms generated using identical formation and borehole parameters but with different borehole radii R .

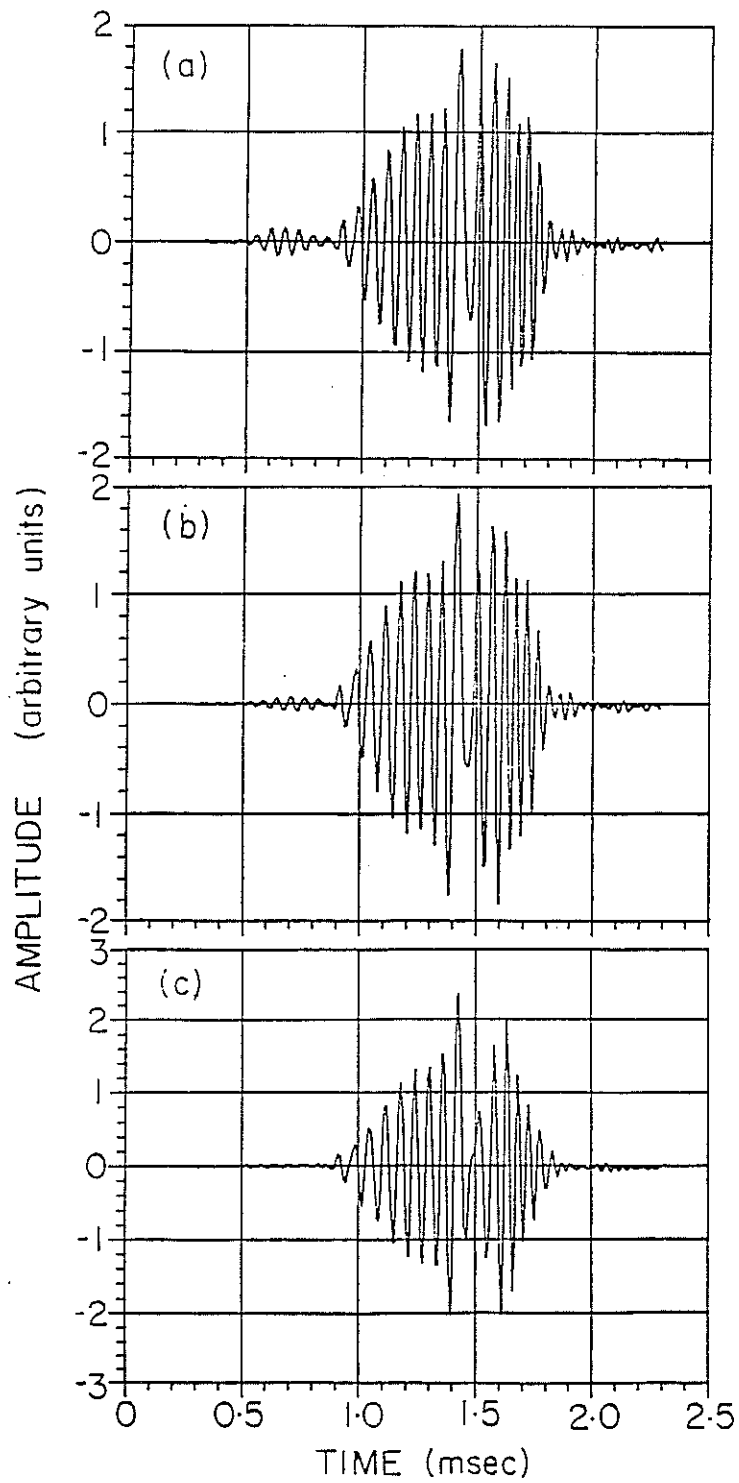


Figure 6: Synthetic microseismograms generated using different Poisson's ratio σ in the formation. (a) $\sigma = 0.32$; (b) $\sigma = 0.26$; (c) $\sigma = 0.10$.

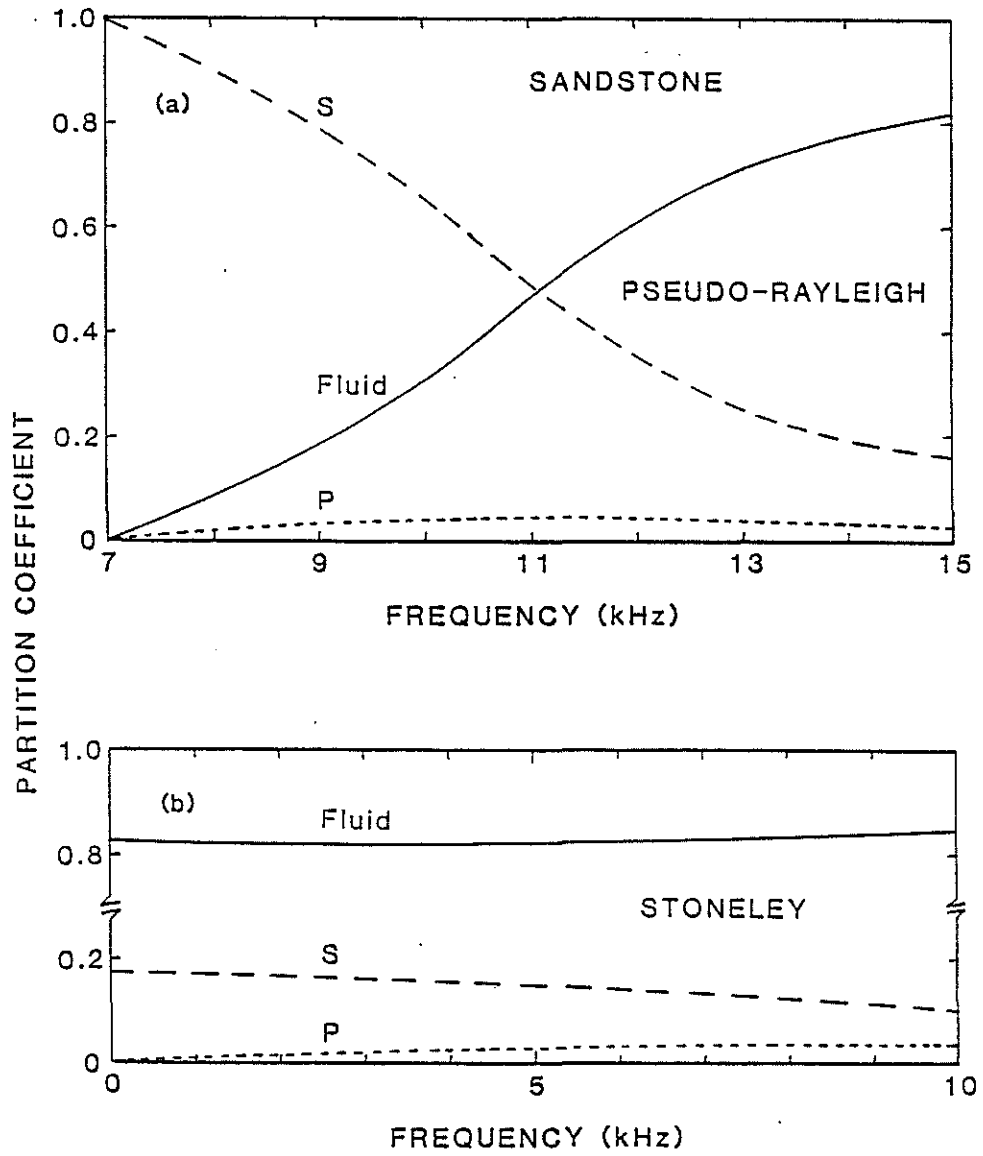


Figure 7: Partition coefficients for (a) the first mode of the pseudo-Rayleigh wave; and (b) the Stoneley wave in a typical sandstone formation.

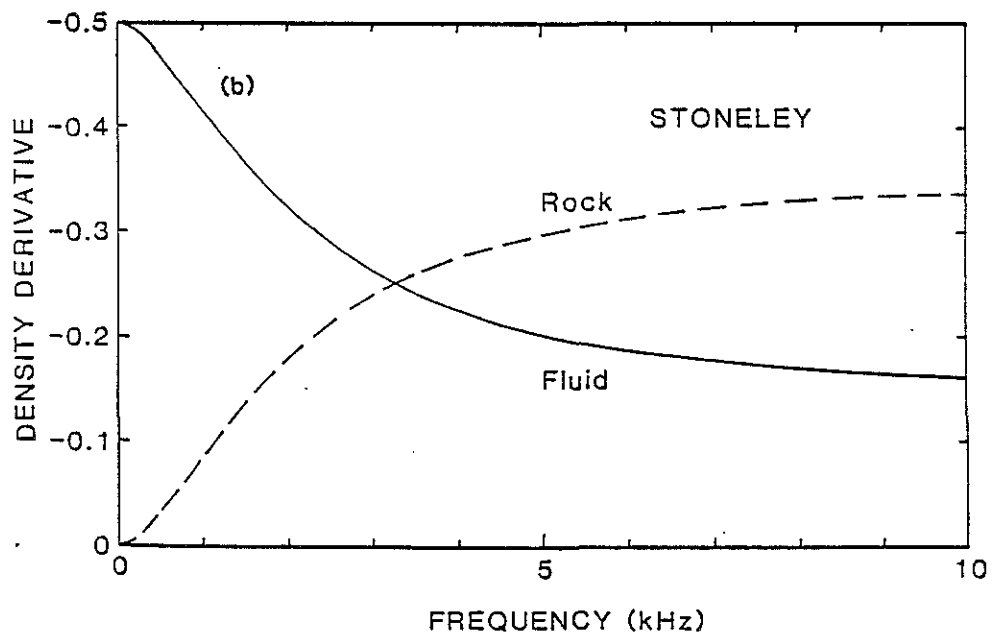
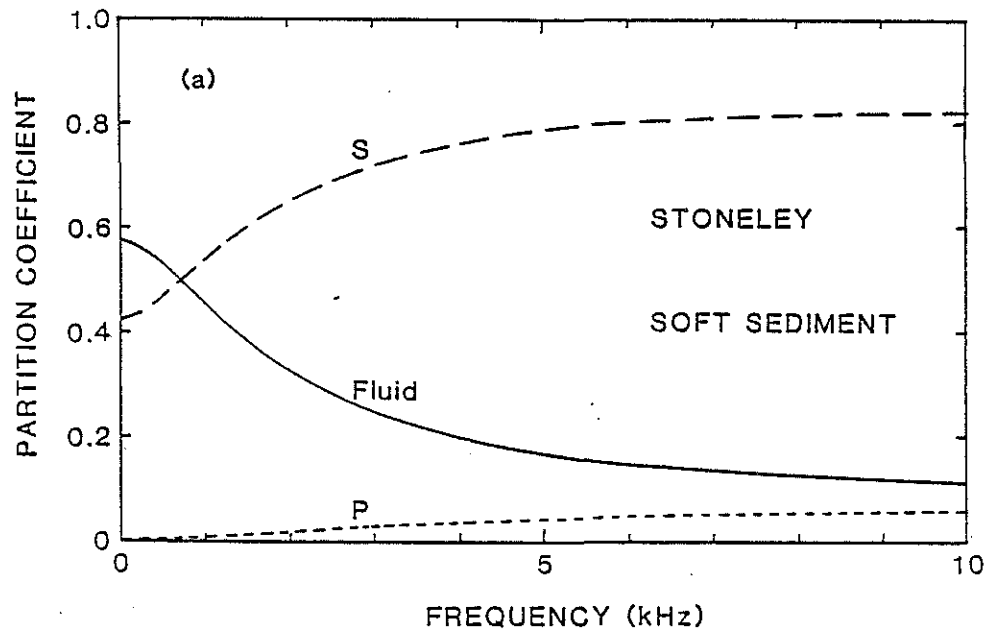


Figure 8: (a) Partiton coefficients; and (b) density derivatives for the Stoneley wave in a typical sediment.

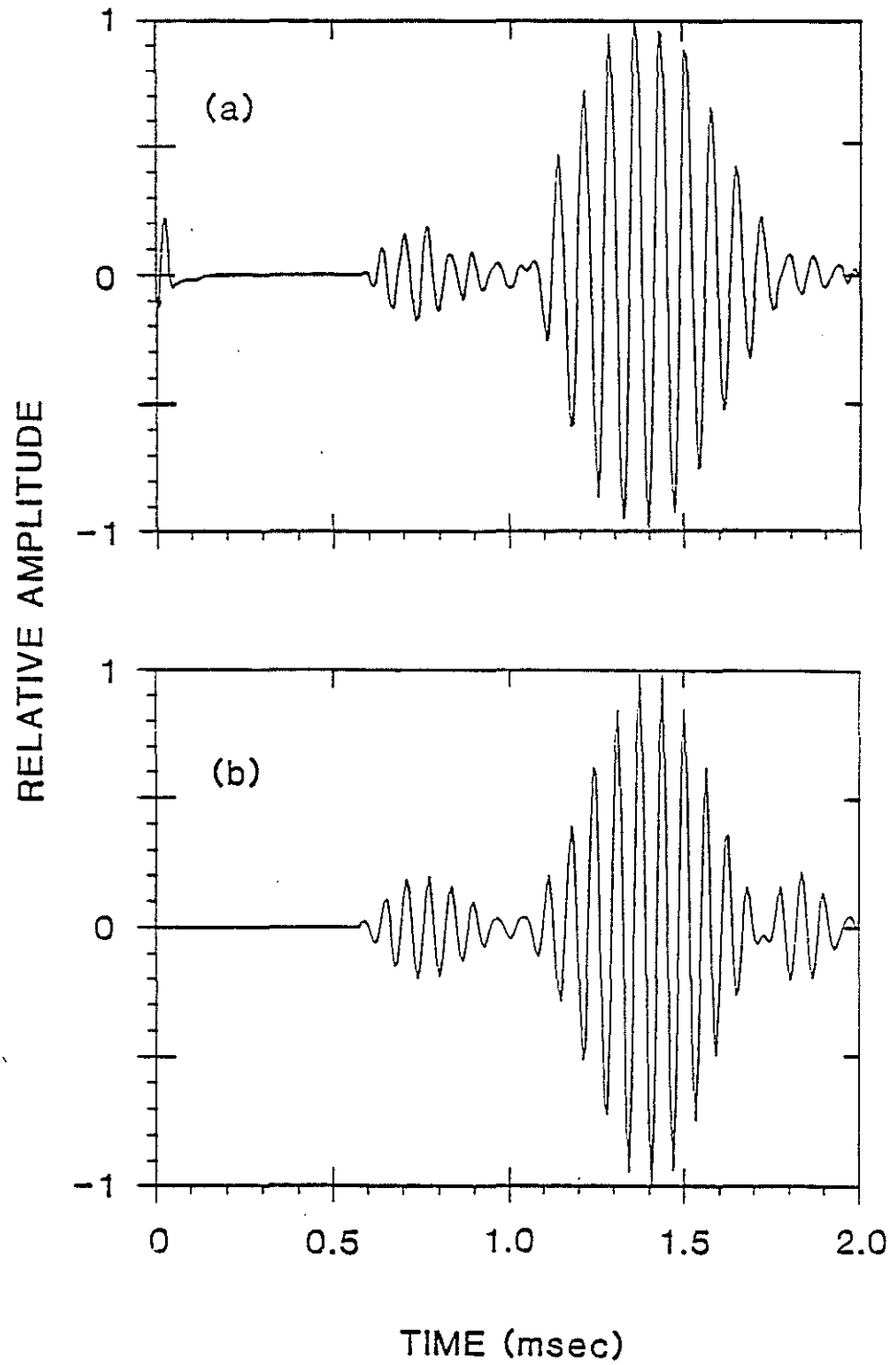


Figure 9: Comparison between (a) actual; and (b) synthetic full waveform acoustic log microseismograms in a limestone formation.

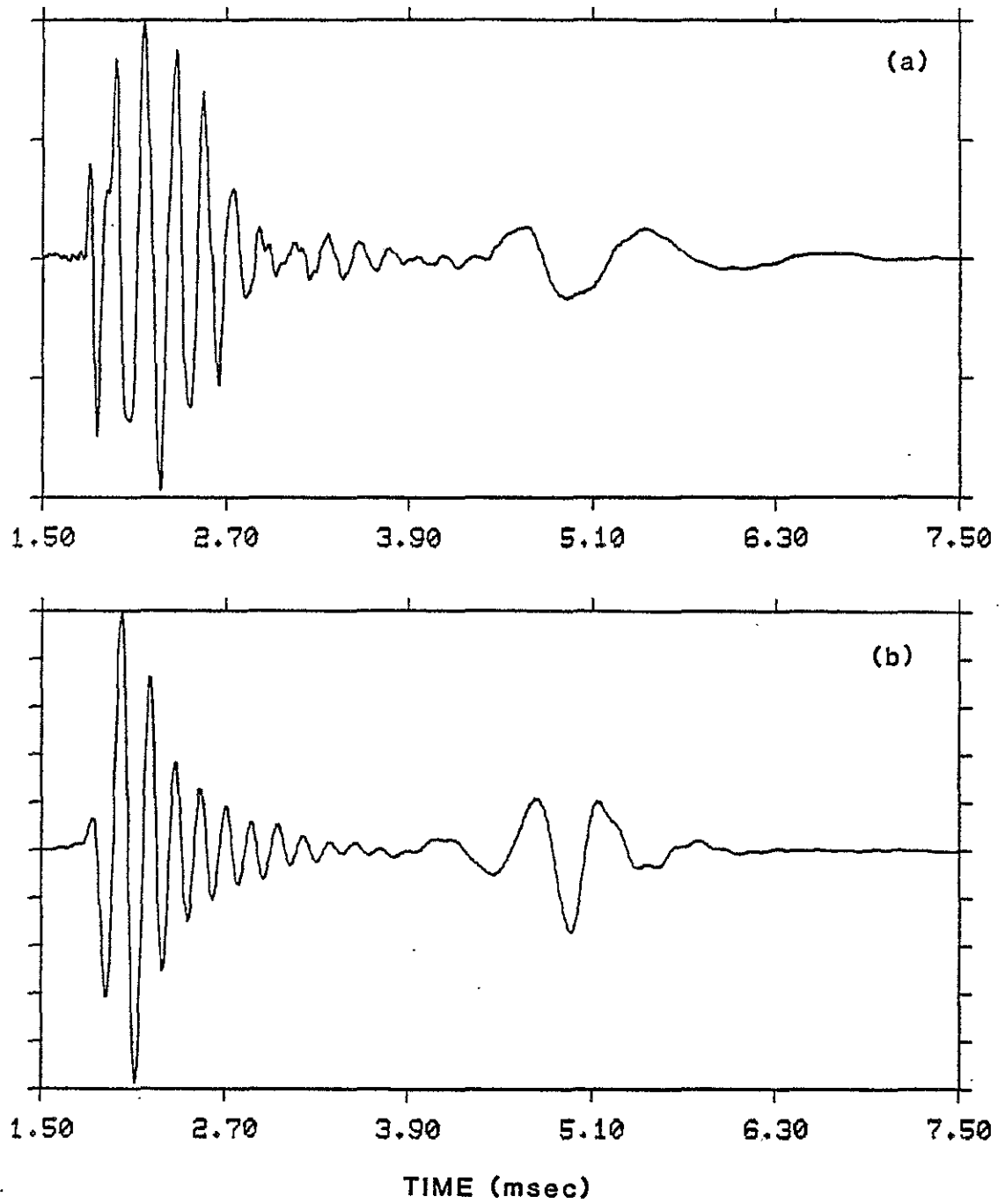


Figure 10: Comparison between (a) actual; and (b) synthetic full waveform acoustic log microseismograms in a "slow" formation.